Microbiological Research 285 (2024) 127744

Contents lists available at ScienceDirect

Microbiological Research

journal homepage: www.elsevier.com/locate/micres

Virulence phenotypes differ between toxigenic *Vibrio parahaemolyticus* isolated from western coasts of Europe

Marion Sorée [a], Solen Lozach [b], Natacha Kéomurdjian [a], David Richard [a], Alexandra Hughes [c], Christine Delbarre-Ladrat [a], Véronique Verrez-Bagnis [a], Alain Rincé [d], Delphine Passerini [a], Jennifer M. Ritchie [c,*], Dominique Hervio Heath [b,*]

[a] *Ifremer, MASAE, Nantes F-44311, France*
[b] *Ifremer, Univ Brest, CNRS, IRD, LEMAR, Plouzané F-29280, France*
[c] *Faculty of Health and Medical Sciences, University of Surrey, Guildford, Surrey, United Kingdom*
[d] *Biotargen, Université de Caen Normandie, Saint-Contest F-14380, France*

ARTICLE INFO

Keywords:
Vibrio parahaemolyticus
Shellfish
Hemolysin
Animal models

ABSTRACT

Vibrio parahaemolyticus is the leading bacterial cause of gastroenteritis associated with seafood consumption worldwide. Not all members of the species are thought to be pathogenic, thus identification of virulent organisms is essential to protect public health and the seafood industry. Correlations of human disease and known genetic markers (e.g. thermostable direct hemolysin (TDH), TDH-related hemolysin (TRH)) appear complex. Some isolates recovered from patients lack these factors, while their presence has become increasingly noted in isolates recovered from the environment. Here, we used whole-genome sequencing in combination with mammalian and insect models of infection to assess the pathogenic potential of *V. parahaemolyticus* isolated from European Atlantic shellfish production areas. We found environmental *V. parahaemolyticus* isolates harboured multiple virulence-associated genes, including TDH and/or TRH. However, carriage of these factors did not necessarily reflect virulence in the mammalian intestine, as an isolate containing TDH and the genes coding for a type 3 secretion system (T3SS) 2α virulence determinant, appeared avirulent. Moreover, environmental *V. parahaemolyticus* lacking TDH or TRH could be assigned to groups causing low and high levels of mortality in insect larvae, with experiments using defined bacterial mutants showing that a functional T3SS1 contributed to larval death. When taken together, our findings highlight the genetic diversity of *V. parahaemolyticus* isolates found in the environment, their potential to cause disease and the need for a more systematic evaluation of virulence in diverse *V. parahaemolyticus* to allow better genetic markers.

1. Introduction

Vibrio parahaemolyticus, a common halophilic bacterial species that inhabits estuarine and marine environments, is the leading bacterial cause of infection associated with the consumption of raw or undercooked seafood worldwide (Su and Liu, 2007). Historically most cases of human infection have been reported in tropical and sub-tropical regions (Nair et al., 2007; Pan et al., 1997). However, climate-driven increases in seawater temperature have contributed to the global expansion of *Vibrio*-related illnesses in temperate regions (Baker-Austin et al., 2013; Deter et al., 2010; Martinez-Urtaza et al., 2018; Vezzulli et al., 2013). The prevailing dogma asserts that not all *V. parahaemolyticus* strains are pathogenic; however, correlations between genetic markers for virulence and clinical infections are not straightforward (Froelich and Noble, 2016).

Early studies identified an association between human infection and strains that exhibit hemolytic activity on Wagatsuma's media, a phenotype commonly known as the Kanagawa phenomenon and attributed to the production of thermostable direct hemolysin (TDH) encoded by the *tdh* gene. Five variants of *tdh* (*tdh1-tdh5)* have been reported with 96–99% nucleotide similarity (Baba et al., 1991; Nishibuchi and Kaper, 1990; Sakurai et al., 1973). TDH-related hemolysin (TRH) producing strains have also been described, and while these isolates appear Kanagawa negative, they have also been linked to disease (Honda et al., 1988; Kishishita et al., 1992). TRH, encoded by the *trh* gene, exists as two variants, *trh1* and *trh2*, which share 84% nucleotide

* Corresponding authors.
E-mail addresses: j.ritchie@surrey.ac.uk (J.M. Ritchie), Dominique.Hervio.Heath@ifremer.fr (D.H. Heath).

https://doi.org/10.1016/j.micres.2024.127744
Received 2 October 2023; Received in revised form 19 April 2024; Accepted 30 April 2024
Available online 6 May 2024

similarity (Kishishita et al., 1992). Previously, TDH and/or TRH producing strains were rarely recovered from the environment (Nair et al., 2007). However, in recent years a number of studies have documented the isolation of TDH and/or TRH-producing isolates from shellfish, seawater or sediments (Bacian et al., 2021; Hazen et al., 2015; Hervio-Heath et al., 2002; Jones et al., 2012; Wagley et al., 2008). Concomitantly, non-TDH/TRH-producing isolates have been recovered from patients (Bhoopong et al., 2007; Jones et al., 2012; Ottaviani et al., 2012; Xu et al., 2015). Consequently, the factors that equate to species pathogenicity have become less clear, further complicated by the discovery that *V. parahaemolyticus* harbours an extensive arsenal of attributes which may affect *V. parahaemolyticus* virulence. This arsenal includes two type six secretion systems (T6SS), various adhesins and toxins (e.g. ZOT, HlyA), and two type three secretion systems (T3SS), located on chromosome 1 (T3SS1) and chromosome 2 (T3SS2) (Makino et al., 2003). Notably, while T3SS1 has been detected in all *V. parahaemolyticus*, this is not the case for T3SS2; the two recognised clades, T3SS2α and T3SS2β, are found in *trh*$^{-}$ and *trh*$^{+}$ isolates, respectively (Park et al., 2000).

Most research has focused on the *tdh*$^{+}$ (*trh*$^{-}$) O3:K6 pandemic reference isolate RIMD2210633 (Makino et al., 2003). Less is known about the pathogenic properties of *trh*$^{+}$ isolates although the emergence of genetic variants of clinical relevance has occurred. For example, the highly pathogenic ST36 clonal group came to the fore in 2012 following disease outbreaks in the Pacific Northwest, the Northeast coast of the United States, and the Northwest coast of Spain (Martinez-Urtaza et al., 2018). Epidemiological data suggest that *trh*$^{+}$ strains have higher attack rates and cause more severe disease (Martinez-Urtaza et al., 2016; McLaughlin et al., 2005), although their pathogenic mechanisms remain less well explored (Raghunath, 2014), in part hindered by a paucity of data from mammalian models.

Several *in vivo* models have been used to study *V. parahaemolyticus* infection. The enterotoxic nature of *V. parahaemolyticus* infection was first demonstrated using rabbit ileal loops, where roles for *tdh* and T3SS2α were uncovered (Hiyoshi et al., 2010; Park et al., 2004). Conversely, intraperitoneal infections in mice revealed role(s) for T3SS1 in systemic infection (Hiyoshi et al., 2010; Pineyro et al., 2010). Gut microbiota-based colonisation resistance limits murine oral infection studies although models based on antibiotic pre-treatment or germ-free mice have recently been described (Yang et al., 2019). However, microbiota loss could create a bias in deciphering *V. parahaemolyticus* pathogenicity as it was recently shown that microbiota appear to play a role in augmenting *V. parahaemolyticus* infection (Wang et al., 2020). Infant rabbits are susceptible to oral infection of *V. parahaemolyticus* and use of this host has revealed insights into the pathological changes that occur during the course of infection for RIMD2210633 (Ritchie et al., 2012) and identified roles for effectors involved in intestinal pathology and colonisation (Hu et al., 2021; Zhou et al., 2013, 2012). Non-mammalian model hosts such as wax moth (*Galleria mellonella*) larvae offer an alternative system for deciphering virulence (Champion et al., 2016). While infection of larvae revealed a putative role for *mutT*, a gene coding for a nudix hydrolase, in TDH/TRH-negative strains (Wagley et al., 2018), the impact of hemolysin(s) or the T3SSs has not been assessed.

The purpose of this study was to examine the diversity and pathogenic capability of *V. parahaemolyticus* isolates collected from the environment of European Atlantic shellfish production areas. Whole genome sequencing and comparative analysis was used to explore the genetic diversity of the species whereas pathogenic capability was assessed using a mammalian infection model and an insect larvae mortality model. When taken together, our findings highlight gaps in knowledge about the food safety risk posed by *V. parahaemolyticus* isolates found in the shellfish environment and the virulence mechanisms that underpin their ability to cause disease.

2. Materials and methods

2.1. Bacterial strains

Eleven *V. parahaemolyticus* isolates were selected based on sampling date, location and origin from a larger collection of mainly environmental isolates obtained over a 15-year period to provide a diverse group of organisms for subsequent genetic analysis (Table 1). These isolates were designated IFVp. In addition, eight previously sequenced *V. parahaemolyticus* genomes were obtained from the NCBI database (hereafter designated NCBI genomes): five clinical isolates (RIMD2210633 (Makino et al., 2003), ATCC 17802 (Yang et al., 2015), CDC_K4557 (Ludeke et al., 2015), MAVP-Q (Xu et al., 2017) and VN-0028 (NCBI 2015)) and three environmental isolates (FORC_014 (Ahn et al., 2016), FDA_R31 (Ludeke et al., 2015), and BB22OP (Jensen et al., 2013)) for genetic comparisons. The NCBI genomes were selected based on having complete genomes (except for VN-0028) and distinct *tdh/trh* gene profiles. For the infection experiments in *G. mellonella*, the following previously described deletion mutants of RIMD2210633 were used: Δ*tdhAS* (aka POR1), ΔT3SS1 (Δ*vscN1*), ΔT3SS2 (Δ*vscN2*) and the triple mutant (aka POR3, Δ*tdhAS* Δ*vcrD1* Δ*vcrD2*) (Hiyoshi et al., 2010).

2.2. Whole-genome sequencing (WGS), assembly, and annotation

IFVp strains for WGS were initially grown on Luria-Bertani agar containing 3% NaCl (LBS) at 37°C for approx. 18 h, prior to the aseptical transfer of a single colony into 1.5 mL of peptone buffered-water (PBW: 20 gL^{-1} of peptone, 20 gL^{-1} of sodium chloride) and subsequent incubation with shaking for 18 h at 37°C. DNA was extracted from the bacterial cells using the GenElute™ Bacterial Genomic DNA kit (Sigma-Aldrich, UK) following manufacturer's recommendations. The purity and concentration of extracted DNA was assessed from 260/280 nm readings taken using the Epoch™ Microplate Spectrophotometer (Bio-Tek, USA). DNA integrity was verified by electrophoresis with a 2% agarose gel. DNA extracts were sent to the GATC platform (Eurofins, France) for sequencing (Illumina HiSeq 4000 type paired-end (2×150bp) 450 bases, approximately 5 million read pairs and 100X average coverage).

Quality of reads was verified using FastQC v0.11.5 and reads were mapped using Bowtie2 (Langmead et al., 2019). The sequences were assembled using Velvet *de novo* v1.2.10 (Zerbino and Birney, 2008). The two chromosome sequences were determined by alignment against the *V. parahaemolyticus* RIMD2210633 reference strain using Mauve Aligner (Rissman et al., 2009) and visualized using BRIG v0.95 (Alikhan et al., 2011). Genome annotation was performed with the interface Magnifying Genomes (MaGE) of the MicroScope web-based service from GenoScope (Vallenet et al., 2009). The sequence type (ST) of each genome was determined using PubMLST (https://pubmlst.org/organisms/vibrio-parahaemolyticus) using seven loci (*dnaE, gyrB, recA, dtdS, pntA, pyrC, tnaA*) (Jolley et al., 2018).

2.3. Core and accessory genome analyses

Prokka v1.14.6 (Seemann, 2014) was used to collect GFF format using Fasta files of the 19 *V. parahaemolyticus* genomes (11 IFVp and 8 NCBI). Roary v3.13.0 (Page et al., 2015) was used to analyse the total core and accessory genomes of *V. parahaemolyticus* strains. Core genes were defined as those present in all strains and accessory genes are those absent in at least one strain. The "Pan/Core-Genome" tool from Microscope platform was used to determine accessory gene numbers (sum of variable and strain-specific genes) present in each strain (Vallenet et al., 2009). Software packages were used under default settings. The core-alignment, generated by Roary, was used to construct a maximum-likelihood phylogeny using RaxML v8.2.4 (Stamatakis, 2014) with a general time reversible gamma model and 100 bootstrap values.

Sequences of *tdh* and *trh* from 14 *V. parahaemolyticus* genomes (eight

Table 1
Characteristics of *V. parahaemolyticus* strains used in this study.

Strain	Isolation year	Country	Source	Sequence type (ST)	Serotype	Ref
IFVp5	2004	France	Clinical	3	O3:K6	This study
IFVp18	1999	France (Atlantic coast)	E (mussel, *Mytilus edulis*)	2581	O2:KUT	This study
IFVp22	1999	France (English Channel)	E (mussel, *M. edulis*)	987	O2:KUT	This study
IFVp69	2002	France (Atlantic coast)	E (mussel, *M. edulis*)	2935	O3:KUT	This study
IFVp136	2004	Portugal (Atlantic coast)	E (mussel, *Mytilus galloprovincialis*)	73	O11:KUT	This study
IFVp177	2006	Portugal (Atlantic coast)	E (oyster, *C. gigas*)	1584	O11:KUT	This study
IFVp182	2005	France (Atlantic coast)	E (seawater)	1294	O11:KUT	This study
IFVp195	2010	France (Atlantic coast)	E (seawater)	1140	O4:KUT	This study
IFVp201	2009	France (Atlantic coast)	E (mussel, *M. edulis*)	2942	O5:KUT	This study
IFVp203	2009	France (Atlantic coast)	E (mussel, *M. edulis*)	2942	O5:KUT	This study
IFVp408	2014	France (Atlantic coast)	E (oyster, *Crassostrea gigas*)	1140	O4:K37	This study
RIMD2210633	1996	Japan	Clinical	3	O3:K6	(Makino et al., 2003)
CDC_K4557	2007	USA	Clinical	799	O1:K33	(Ludeke et al., 2015)
VN-0028	1995	Germany	Clinical	966	UNK	(NCBI 2015)
MAVP-Q	2011	USA	Clinical	631	UNK	(Xu et al., 2017)
FORC_014	2015	South Korea	E (toothfish)	1629	UNK	(Ahn et al., 2016)
BB22OP	1980	Bangladesh	E	88	O4:K8	(Jensen et al., 2013)
FDA_R31	2007	USA	E (oyster)	23	O1:KUT	(Ludeke et al., 2015)
ATCC 17802	1951	Japan	Clinical	1	O1:K1	(Yang et al., 2015)

E: environmental, KUT: K untypable, UNK: unknown

IFVp and six NCBI genomes) and six NCBI hemolysin reference sequences (two *trh* and four *tdh* sequences) were aligned using MUSCLE and a minimum evolution (ME) phylogeny with 1000 bootstrap was constructed using MEGA X (Kumar et al., 2018). This analysis involved 26 amino acid sequences. Tree was annotated using Interactive Tree of Life (iTOL v6) (http://itol.embl.de). Pathogenicity islands VPaI-1 to VPaI-6, characterized in RIMD2210633 (Hurley et al., 2006), were determined using BLASTp. VPaI-7, which was composed of the T3SS2 cluster and *tdh/trh* hemolysin genes, was identified using the Microscope platform "Regions of Genome Plasticity" (RGP) tool (Vallenet et al., 2009). *In silico* identification of known virulence genes was performed using BLAST+ v2.11.0 (Camacho et al., 2009). Genes identified in this study were *tdh1 to 4* (Nishibuchi and Kaper, 1985, 1990), *trh1* and *trh2* (Kishishita et al., 1992; Nishibuchi et al., 1989), T3SS1 and T3SS2 (Makino et al., 2003; Okada et al., 2009), T6SS1 and T6SS2 (Salomon et al., 2013), phage f237 (Nasu et al., 2000), biofilm *bcs* cluster (Meparambu Prabhakaran et al., 2022) and toxins encoded by *zot* (Perez-Reytor et al., 2020) and *hlyA* (VCA0219) genes.

The relationships between accessory gene presence-absence and (i) origin (*i.e.* clinical and environmental), (ii) *tdh* presence-absence and (iii) *trh* presence-absence were investigated using Scoary v1.6.16 (Brynildsrud et al., 2016). For these analyses, the gene presence-absence matrix, generated by Roary, and a binary matrix indicating the traits of each strain were used. Pairwise comparisons were deemed significant when the Benjamini-Hochberd adjusted *p*-values were less than 0.05.

2.4. Infant rabbit experiments

All experimental protocols were approved by the local Animal Welfare and Ethical Review Body, the Home Office and carried out in accordance with the UK Animals (Scientific Procedures) Act 1986. Timemated adult New Zealand White female rabbits were obtained from a commercial breeder (Harlan Laboratories, UK). Experiments were performed on individual litters of 2–3 days old infant rabbits that were housed as a group in a nest box with the lactating doe for the duration of the study. Infections with the two test *V. parahaemolyticus* strains (IFVp201 and IFVp195) were performed on animals derived from at least two independent litters to counter reporting of litter-specific effects. Low birth weight rabbits < 40 g bodyweight were removed as these animals tend to exhibit different disease kinetics. Otherwise, all animals within a litter were infected and euthanised at either 15, 38 or 120 h post infection (HPI).

Experiments were performed as described (Ritchie et al., 2012), except animals were pre-treated with the histamine H_2-receptor antagonist, ranitidine (5 $mgkg^{-1}$ bodyweight via intraperitoneal injection; GlaxoSmithKline), 3 h prior to orogastric inoculation to transiently increase stomach pH. *V. parahaemolyticus* inoculum was prepared from stationary phase cultures grown with shaking in tryptone soy broth (TSB) at 37°C for 18 h. For IFVp201, TSB or tryptone soy agar (TSA) was supplemented with carbenicillin (50 μg mL^{-1}). Cells were collected by centrifugation (5 min at 5000 g) and the cell pellet resuspended in sodium bicarbonate solution (2.5 g in 100 mL; pH 9) to give a final concentration of $\sim 1\times10^{9}$ CFU mL^{-1}. Rabbits were orogastrically inoculated using a size 4 French catheter at a dose equivalent to 0.5 mL per 90 g rabbit bodyweight and then after monitored frequently for signs of disease. Disease was recorded when visible signs of solid or liquid faecal contamination were observed on the anus or ventral surface of the rabbits; healthy rabbits remained clean with no signs of contamination. At the indicated time points, rabbits were humanely killed and the entire intestinal tract from the duodenum to the rectum was removed and processed to determine levels of fluid accumulation and *V. parahaemolyticus* colonisation. Fluid accumulation ratios (FAR) were obtained by determining the weight of fluid present in a section of the distal small intestine divided by the entire weight (fluid and tissue) of the section. Concentrations of *V. parahaemolyticus* (in log $CFUg^{-1}$) were determined in tissue samples taken from the proximal (I1), mid (I2) and distal (I3) regions of the small intestine. Tissue samples were homogenised between two glass slides using 2 mL sterile PBS prior to serial dilution and plating on TSA. Colonies were confirmed as *V. parahaemolyticus* following growth on thiosulfate-citrate-bile salts-sucrose (TCBS) agar. For some rabbits, the internal organs including the gall bladder, spleen and liver were also collected, homogenized and plated on selective media to check for systemic spread of *V. parahaemolyticus*.

2.5. Galleria mellonella larvae experiments

Pathogenicity of RIMD2210633 mutants and IFVp strains were evaluated using *G. mellonella*, with minor differences in inoculum preparation due to the work being performed in different laboratories. RIMD2210633 derived mutants were grown on TSA and incubated at 37°C for 24 h. Following growth, 1–2 discrete colonies were inoculated into 5 mL TSB and incubated with shaking at 37°C for 18 ± 2 h. The resulting cell suspensions were centrifuged to remove spent media,

washed once in an equivalent volume of PBS and then adjusted with PBS to yield a final concentration of ~1×10^7 CFU mL^{-1}. IFVp strains were initially grown on Heart Infusion (DIFCO ™, USA) agar containing 0.5% NaCl (HIS) at 37°C for 24 h, prior to aseptically transfer of a single colony into 20 mL of HIS broth and subsequent incubation with shaking for 8 h at 37°C. After incubation, cultures were washed twice and diluted with buffered-physiological water (BPW: 0.4 g L^{-1} of $K_2H_3PO_4$; 4.5 g L^{-1} of Na_2HPO_4, 12 H_2O; 7.2 g L^{-1} of NaCl) to obtain a *V. parahaemolyticus* inoculum with final concentration of 5×10^6 CFU mL^{-1} (confirmed by plate enumeration onto HIS at 37°C for 24 h).

G. mellonella infections with RIMD2210633 mutants were performed at the University of Surrey (United Kingdom) while *G. mellonella* infections with IFVp strains were performed in IFREMER laboratories (Brest, France). In both laboratories, larvae of *G. mellonella* measuring 2–3 cm in body length (body weight of approx. 200–300 mg) were used. For each experiment, 10 μL of *V. parahaemolyticus* inoculum (~ 5×10^4 CFU of bacteria) was injected into the right foremost pro-leg of larvae using a syringe pump (KD Scientific, USA). Control groups (n = 20) were inoculated with PBS or BPW in the same conditions. Larvae were maintained in Petri dishes at 37°C in the dark. All larvae were monitored for 24 h and percentage survival determined. Larvae that did not respond to touch were scored as dead. Three independent infection experiments were performed for each *V. parahaemolyticus* strain. Data represent the mean survival (± standard error) of three independent experiments each consisting of 20 larvae per group.

Determination of LD_{50} was performed on a subset of strains as described above by larvae injection with concentrations of *V. parahaemolyticus* inoculum ranging from 5×10^2 to 5×10^6 CFU of bacteria. Mortality was recorded at 24 HPI. LD_{50} was calculated as the concentration inducing 50% mortality and was expressed in CFU mL^{-1}.

2.6. Statistical analyses

All statistical analyses of the data were performed using RStudio 2021.09.0+351 "Ghost Orchid" Release (2021–09–20) for Windows or in GraphPad Prism (version 8.4.3). Data are presented as means ± standard error and the significance level was set to $p < 0.05$. The following statistical analyses were performed to compare IFVp201 and IFVp195 infection parameters in rabbits; proportion of infected rabbits (Fisher's exact test), fluid accumulation ratios (unpaired two-tailed Student t-test) and *V. parahaemolyticus* concentrations (unpaired two-tailed Student t-test). Percentages of larvae survival during bacterial infections between RIMD22210633 and its mutants, and between IFVp strains were evaluated using one way ANOVA with strain as a factor, followed by Tukey honest significant differences post hoc test to determine where differences occur.

2.7. Genome accession numbers

Draft genomes of the *V. parahaemolyticus* strains are available from the European Nucleotide Archive (Project ID: PRJEB53525) under the accession numbers shown in Table S1.

3. Results

3.1. Source and genetic properties of V. parahaemolyticus

Eleven IFVp isolates, originally sourced from shellfish (n=8), seawater (n=2) and from a clinical case (n=1), were subject to WGS and their sequences compared to 8 previously published *V. parahaemolyticus* genomes from NCBI, chosen to reflect the diversity within the species. Within the IFVp collection, seven serotypes, and 9 STs based on multilocus sequencing typing (MLST) including 2 that were novel (ST2935 and ST2942), were detected (Table 1). One strain, IFVp5, exhibited the same ST as the pandemic reference strain RIMD2210633 (ST3). The IFVp draft genomes ranged in size from 4.9 to 5.4 Mb with a GC content of 45.1–45.6% and contained on average 3223 and 1888 Kb in chromosomes 1 and 2, respectively (Table S1). A total of 4715 to 5420 coding sequences (CDS) per genome were predicted. One strain, IFVp182, contained a 40.2 Kb plasmid encoding 45 CDS including genes for a type IV secretion system, similar to the plasmid found in FORC_014 (Ahn et al., 2016).

The pan genome of the 19 *V. parahaemolyticus* genomes comprised of 9161 coding genes including 3616 (39%) core genes and 5545 (61%) accessory genes. The number of accessory genes ranged from 915 to 1800 per strain (Table S2). Our results showed that the number of *V. parahaemolyticus* genes in the pan genome increased (Fig. 1A) and the number of new core genes decreased (Fig. 1B) with the addition of each *V. parahaemolyticus* genome. This suggests *V. parahaemolyticus* has an open pan genome. Phylogenetic analysis based on core genomes demonstrated that the isolates were genetically diverse and clustered according to sequence type *e.g.* clinical strain IFVp5 (*tdh1*$^+$ *tdh2*$^+$) and RIMD2210633 (*tdh1*$^+$ *tdh2*$^+$), are both ST3 (Fig. 1C).

Next, we examined if genes associated with the previously described filamentous phage f237 were restricted to O3:K6 and closely related serovars (Iida et al., 2001; Nasu et al., 2000). Phage f237 contains 10 ORFs, including ORF7 that encodes the ZOT toxin. BLAST analysis revealed that ORF1 to ORF7 were present in four non-O3:K6 genomes at >97% homology (FDA_R31, IFVp18, IFVp136 and IFVp203) (Fig. S1). ORF8, the f237 target gene, was missing in all strains whereas ORF9 was present at 90–95% of homology in the previously mentioned 4 strains, and ORF10 was present at 100% homology in FDA_R31 and 59% homology in the three other strains (IFVp18, IFVp136 and IFVp203). Interestingly, none of f237 ORFs were detected in IFVp5, an O3:K6 clinical isolate.

3.2. Environmental V. parahaemolyticus hemolysin and virulence gene content

To identify the hemolysin variants present in the *V. parahaemolyticus* strains used in this study, four TDH (TDH1 – TDH4) and two TRH (TRH1, TRH2) reference protein sequences were aligned with the annotated protein genomes and a minimum-evolution phylogenetic tree was generated (Fig. S2). Five hemolysin profiles were identified within the IFVp isolates: TDH1 (n=2), TDH1-TDH2 (n=1), TDH3-TRH1 (n=2), TRH1 (n=2), and TRH2 (n=1), while three isolates lacked hemolysins (Table 2). Two TDH variants, TDH2 and TDH3 co-existed with other hemolysins, whereas TRH2 was found alone. FDA_R31 harboured a TDH hemolysin (M634_24535) that shared 89%, 91%, 92% and 92% similarity with *tdh1*, *tdh2*, *tdh3* and *tdh4*, respectively.

Genomic comparisons also revealed that previously described virulence clusters such as the mannose-sensitive hemagglutinin (MSH), chitin-regulated pilus (ChiRP), polar and lateral flagella, T6SS2, and T3SS1 were present in all IFVp strains (Fig. 2). The presence/absence of key virulence factors in relation to each strains' hemolytic profile can be found in Table 2. One isolate, IFVp182, lacked TDH or TRH but contained genes comprising T3SS2α demonstrating that the link between these two virulence determinants, which tend to be co-located on the same pathogenicity region, is not absolute. T6SS1 was present in 12 strains whereas a cellulose secretion operon (*bcs*) was identified in 6 of 7 strains that lacked T6SS1.

We next examined the distribution of the seven genomic islands (VPaI-1–7) (Hurley et al., 2006). BLASTp analysis revealed that VPaI-1 was partially present in IFVp18, IFVp5, CDC_K4557 and VN-0028 and missing in all other strains, except for the presence of a single gene (VP0394) in IFVp177 and FDA_R31. VPaI-2 and VPaI-3 were partially present in all strains, whereas VPaI-4 was partially present only in IFVp18 (Table S3). VPaI-5 was also partially present in IFVp18 and BB22OP, while VPaI-6 could be found in IFVp5, IFVp22, FDA_R31, BB22OP and MAVP-Q. A schematic illustration of VPaI-7, which also contains the T3SS2 cluster, highlighted that VPaI-7 was absent in IFVp18, IFVp69 and CDC_K4557 and that the island's organization

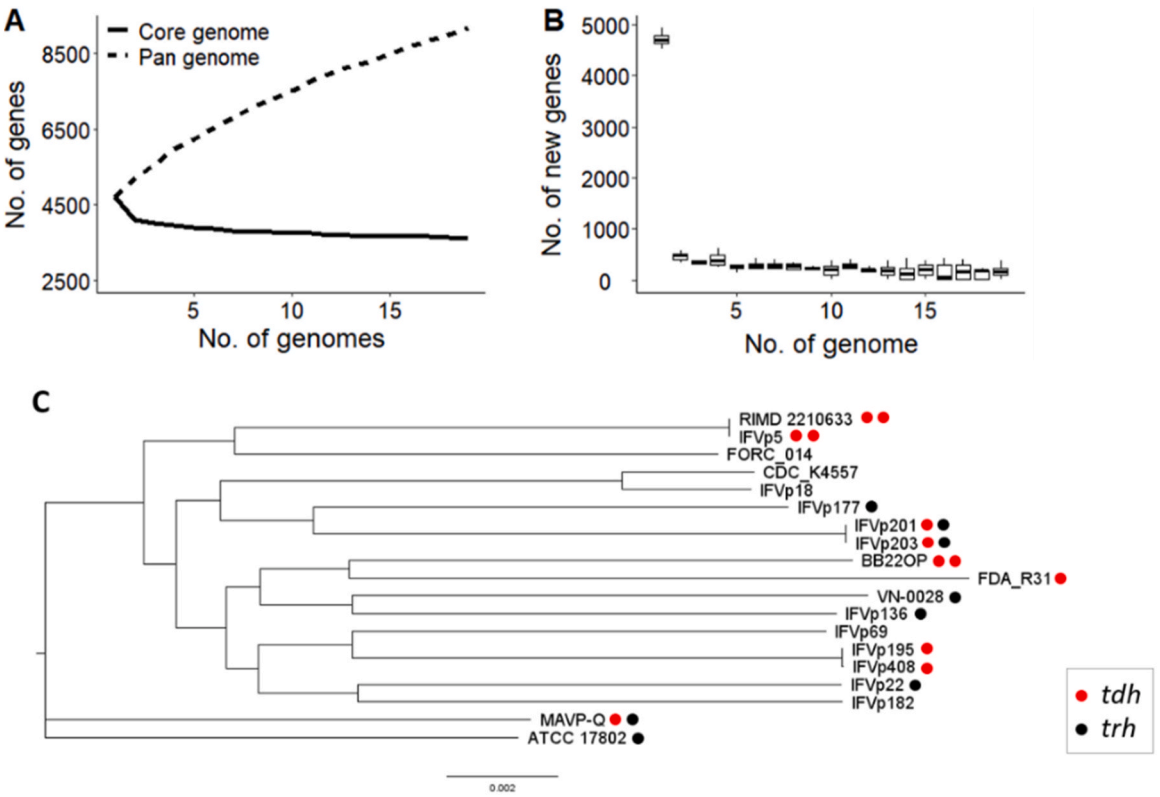

Fig. 1. Pan-genome analysis and core-genome phylogeny of *V. parahaemolyticus* strains. (A) Estimated number of core and pan genes, and (B) number of new genes. (C) Maximum-likelihood tree obtained from concatenated nucleotide sequence alignment of core genes using RaxML with 100 bootstraps.

Table 2
In silico detection of known virulence genes in *V. parahaemolyticus* strains.

Strains	Hemolysins		T3SS		T6SS		Toxins			Biofilm
	tdh	*trh*	T3SS2	T3SS1	T6SS1	T6SS2	ZOT	*hly*	*Toxin B*	*bcs*
IFVp18				+	+	+	+			
IFVp69				+		+				
IFVp182			α	+	+	+				
IFVp195	1		α	+	+	+				
IFVp408	1		α	+	+	+				
IFVp5	1+2		α	+	+	+				
IFVp201	3	1	β	+		+				+
IFVp203	3	1	β	+		+	+			+
IFVp136		1	β	+	+	+	+	+		
IFVp177		1	β	+		+				+
IFVp22		2	β	+	+	+		+	+	
CDC_K4557				+	+	+				
FORC_014			α	+		+				+
FDA_R31	*		β	+		+	+	+		+
RIMD2210633	1+2		α	+	+	+	+			
BB22OP	1+2		α	+	+	+				
MAVP-Q	3	1	β	+		+				+
VN-0028		1	β	+	+	+				
ATCC_17802		2	β	+	+	+		+	+	

* : novel *tdh* variant

varied (Fig. S3). Analysis of genes and clusters present in VPaI-7 showed that a gene encoding the accessory colonization factor D (*acfD*) was located near the T3SS2 gene cluster in all cases. We also confirmed the presence of the urease operon in all *trh*$^+$ strains (Fig. S3). We observed that the gene encoding toxin B, a catalytic glycosyltransferase domain containing protein, was found in *trh2*$^+$ strains while the *hly* operon (*hlyCABD*) was present in only some *trh*$^+$ strains (IFVp136, IFVp22 and ATCC 17802) (Fig. S3; Table 2).

While T3SS1 was present in all 19 *V. parahaemolyticus* strains, we noticed some differences in gene organisation in this region. For example, region VP1676-VP1679 was missing in IFVp201, IFVp203 and FDA_R31 strains (Fig. 3A). This region was replaced by three new genes in IFVp201 and IFVp203: a secretion protein, a MFS transporter and a TetR/AcrR family transcriptional regulator gene, all previously described (Wu et al., 2020). ATCC 17802 harboured three additional genes coding for a N-acetyltransferase, a transporter protein and a LysR family transcriptional regulator, located between VP1679 and *vopQ*. All four previously described T3SS1 effectors, VopQ, VopS, VopR, and VPA0450, were found in all strains.

T3SS2 was present in 16 of 19 strains (missing in IFVp18, IFVp69 and

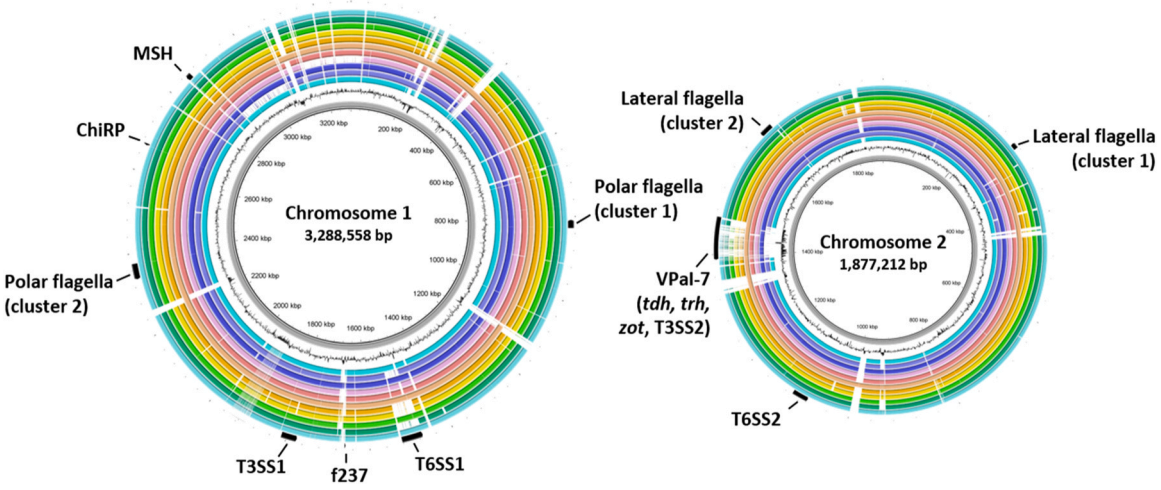

Fig. 2. Comparison of environmental *V. parahaemolyticus* genomes using RIMD2210633 as a reference. Analysis performed by BLASTn using BRIG software. Left: chromosome 1, right: chromosome 2. From the inside out: RIMD2210633 (grey), GC content (black), IFVp18 (light blue), IFVp69 (purple), IFVp182 (dark blue), IFVp195 (light pink), IFVp408 (pink), IFVp5 (light orange), IFVp201 (orange), IFVp203 (yellow), IFVp136 (green), IFVp177 (turquoise) and IFVp22 (light turquoise). Names of previously described virulence clusters are indicated on the external ring; MSH: mannose-sensitive hemagglutinin, ChiRP: chitin-regulated pilus, T3SS: type III secretion system, T6SS: type VI secretion system, VPaI-7: Pathogenicity Island of *V. parahaemolyticus* number 7.

CDC_K4557) (Fig. 3B). Homology heatmaps of the T3SS2 region showed distinct differences in T3SS2α and T3SS2β gene content, and that T3SS2β was concomitant with the presence of the *trh* gene even in *tdh*$^+$ *trh*$^+$ strains. While isolates that encode only *tdh*$^+$ typically harboured the T3SS2α variant, FDA_R31 (*tdh*$^+$ *trh*$^-$) proved an exception and contained genes corresponding to T3SS2β (Fig. 3B). T3SS2 effectors VopC, VopZ, VopP, VopL and VPA1380 were present in all the strains while VopT and VopV were absent in *trh*$^+$ and *tdh*$^+$ *trh*$^+$ strains.

Finally, we used Scoary analysis to look for associations between pan-genome components and phenotypes (Brynildsrud et al., 2016). This analysis failed to detect any genes that were significantly over- or under-represented in the accessory genome of clinical versus environmental strains, or of *tdh*$^+$ versus *tdh*$^-$ strains. However, 51 genes were over-represented in the accessory genome of *trh*$^+$ strains compared to *trh*$^-$ strains including those coding for the urease operon and some genes within the T3SS2 cluster (Table S4).

3.3. Infant rabbit infections

To begin to assess the pathogenic potential of the IFVp isolates, 2–3-day old infant rabbits were orogastrically inoculated with either IFVp201 or IFVp195; strains which harboured contrasting virulence features (IFVp201: *tdh3/trh1*, T3SS2β, T6SS1$^-$ *vs* IFVp195: *tdh1*, T3SS2α, T6SS1$^+$; see Table 2). IFVp201 caused diarrhoea with most rabbits contaminated by liquid faeces from ~12 hours post infection (HPI). By 15 HPI, significant amounts of fluid had accumulated in their small intestines, and between 10^8 and 10^9 CFUg^{-1} could be recovered from this region (Fig. 4). In marked contrast, IFVp195 failed to cause overt diarrhoea or fluid accumulation in the cecum of rabbits even by 120 HPI. Concentrations of IFVp195 were nearly 5 logs lower than those of IFVp201 in all regions of the small intestine at 15 HPI ($p \leq 0.001$), the only time point where direct comparisons were possible. IFVp195 concentrations increased to approximatively 6 log CFUg^{-1} by 38 HPI, then appeared to stabilise. A few animals infected with IFVp201 were found to contain ~10^3 CFUg^{-1} in bile and spleen but cross-contamination from the intestine at the time of organ collection could not be ruled out. Overall, our findings suggest that IFVp201 induced more severe disease and appeared more able to colonise the mammalian intestine than IFVp195.

3.4. Galleria mellonella larvae infections

Prior to testing the IFVp isolates in larvae, we sought to better understand the factors that impact *G. mellonella* mortality (Fig. 5A) using a set of previously described RIMD2210633 mutants (Hiyoshi et al., 2010). While wild type, Δ*tdh*, and ΔT3SS2 mutants were highly virulent killing 100% of larvae, survival was significantly greater in those infected with the ΔT3SS1 (38%) or the triple mutant (20%) (Fig. 5B, $p<0.05$). These findings suggest that a functional T3SS1 plays an important role in *V. parahaemolyticus* virulence in *G. mellonella* larvae infected by injection.

Next, we assessed larval survival following injection of the individual IFVp strains. Larvae survival ranged widely, revealing that four strains (IFVp182, IFVp22, IFVp201 and IFVp203) were poorly virulent (larvae survival > 75%), four strains (IFVp18, IFVp408, IFVp177 and IFVp69) were highly virulent (larvae survival < 15%) while the two remaining strains (IFVp195 and IFVp136) induced an intermediate phenotype (larvae survival ~ 25–30%) (Fig. 6). We determined the LD_{50} of one strain from each category to confirm their relative virulence. LD_{50} values for IFVp201 (4.3×10^5 CFU mL^{-1}), IFVp195 (3.7×10^4 CFU mL^{-1}) and IFVp408 (6.0×10^3 CFU mL^{-1}) (Fig. S4) confirmed their virulence ranking with IFVp408 having the lowest LD_{50} value and IFVp201 the highest. Notably, non-hemolytic strains could be found in both high (IFVp18, IFVp69) and low (IFVp182) virulence groups, respectively.

4. Discussion

Given the marine niche of *V. parahaemolyticus* and filter-feeding behaviour of shellfish, the identification of pathogenic *V. parahaemolyticus* is critical to reduce the risk of infection for seafood consumers. Growing evidence indicates that the presence of classical genetic markers (*i.e. tdh, trh,* T3SS2) no longer accurately reflects pathogenic potential (Jones et al., 2012; Ottaviani et al., 2012). Here, we used *in silico* genetic characterisation and *in vivo* infection models to explore the pathogenic potential of 11 *V. parahaemolyticus* isolates collected from shellfish production areas in the European Atlantic.

The core genome of *V. parahaemolyticus* strains described in our study was slightly smaller than some non-hemolytic strains (Castillo et al., 2018; Ronholm et al., 2016), and slightly larger than O3:K6 pandemic strains (Chen et al., 2011). Core genome phylogenies confirmed strain clustering in accordance to ST (*e.g.* RIMD2210633 and

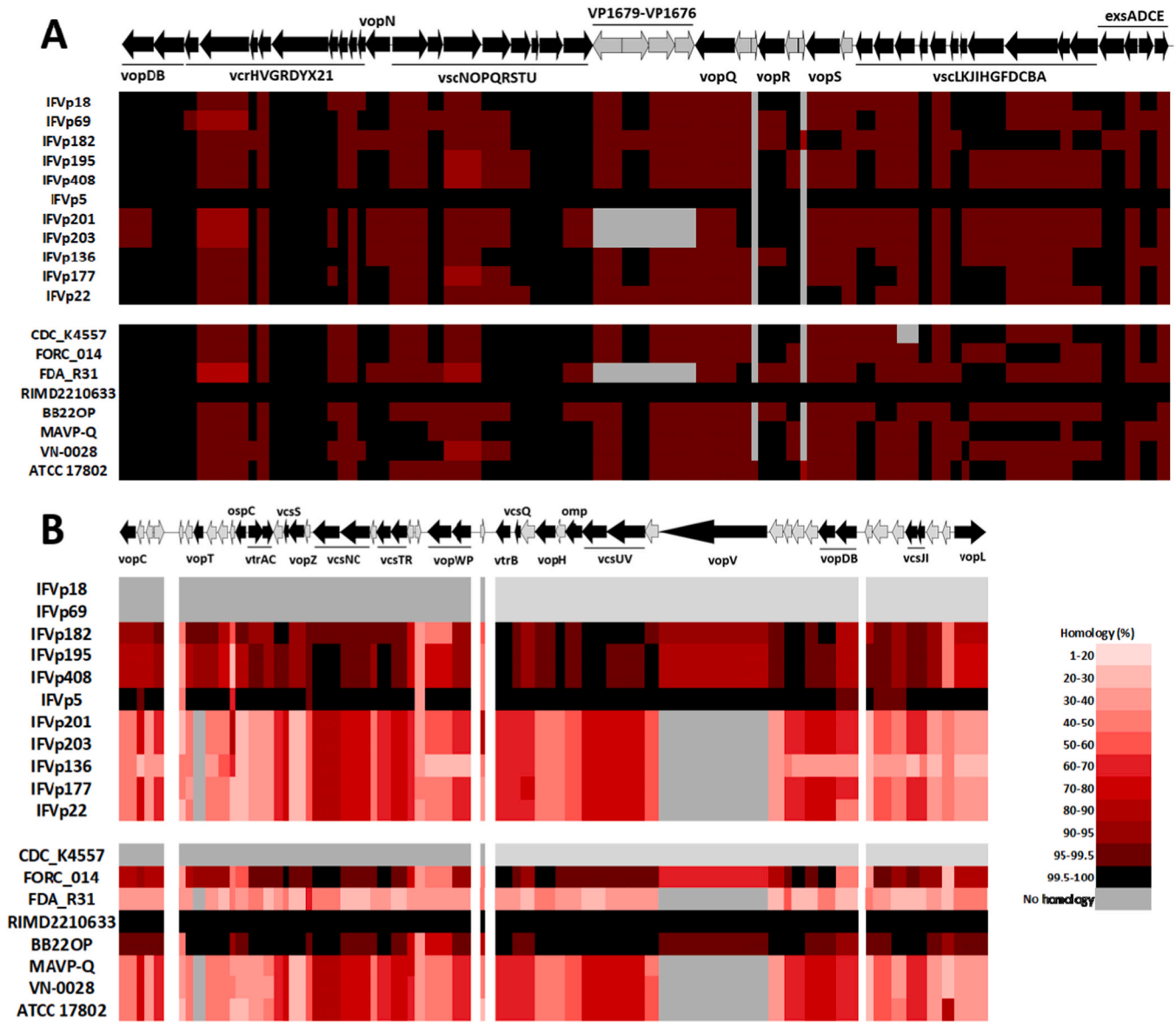

Fig. 3. Heatmaps of the two T3SS clusters in the 19 *V. parahaemolyticus* strains. (A) T3SS1 cluster. (B) T3SS2 cluster. Results are based on BLASTp analyses with RIMD2210633 sequences as reference: T3SS1 (VP1656-VP1702) and T3SS2 (VPA1321-VPA1370). Black arrows: proteins with known function. Grey arrows: proteins with unknown function.

IFVp5, IFVp195 and IFVp408) as previously reported (Jesser et al., 2019; Ronholm et al., 2016). Our findings also demonstrated the open pan genome of the species, which infers gene gain and high rates of horizontal gene transfer that could contribute to increased bacterial fitness (adaptability) in the environment (McInerney et al., 2017).

As has been reported previously, we found that all strains harboured a T3SS1 gene cluster (Hazen et al., 2015), although the organisation of genes within the non-conserved 'effector' region allowed further grouping. Using the groups originally proposed by Wu and colleagues (Wu et al., 2020), our collection contained two strains (IFVp201 and IFVp203) belonging to VPIII where VP1676–1679 are replaced by 3 new genes, one strain (ATCC 17802) belonging to VPII where 3 additional genes are located adjacent to the VP1676–1679 genes, one strain (FDA_R31) with a unique organization not previously described, and the remaining 14 strains belonged to VPI where gene arrangements mirrored that of RIMD2210633. VP1676-VP1679 genes appear to have no impact on the organism's cytotoxicity to mammalian (Ono et al., 2006) or fish cells (Wu et al., 2020), although these genes were significantly upregulated when *V. parahaemolyticus* switched from a smooth to a wrinkly colony morphology (Wu et al., 2022), a physiological state that may aid bacterial growth and survival. Whether the alternative 3-gene cluster contributes to *in vivo* virulence remains to be explored. Moreover, we showed that *G. melonella* survival was greater when larvae were injected with a non-functional T3SS1 mutant of RIMD2210633, suggesting that larvae offer an alternative model for studying the cytotoxic impacts of infection.

Consistent with the findings of other reports (Hazen et al., 2015; Jones et al., 2012), we noted a relationship between T3SS2 and *trh*, *i.e.* the T3SS2β variant co-existed in trh^+ strains (even in tdh^+ trh^+ strains) whereas T3SS2α was found in trh^- strains, with exception of the FDA_R31, which lacks *trh*, harboured T3SS2β and a novel *tdh* variant. All *V. parahaemolyticus* strains carried the T6SS2 gene cluster (Yu et al., 2012) while only 12 of the 19 strains contained T6SS1. T6SS1 may enhance *V. parahaemolyticus* fitness in marine environments by conferring anti-bacterial activity that allows the organism to outcompete other bacteria (Salomon et al., 2013). Interestingly, a cellulose secretion operon (*bcs*) was identified in most strains lacking T6SS1, perhaps providing an alternative survival strategy for these organisms

Bacterial strain (time (h))	IFVp201 15 h	IFVp195 15 h	IFVp195 38 h	IFVp195 120 h
Disease[A]	9/12 (75%)	0/16 (0%)	2/11 (18%)	0/5 (0%)
FAR[B]	0.69 ± 0.44	0.04 ± 0.03	0.07 ± 0.12	0.05 ± 0.05

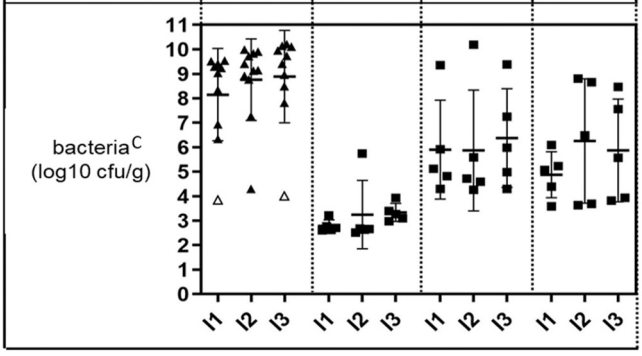

Fig. 4. Kinetics of disease, fluid accumulation and intestinal colonisation of infant rabbits infected with *V. parahaemolyticus* IFVp201 and IFVp195. Infant rabbits were oro-gastrically inoculated with ~5 $\times 10^8$ CFU of IFVp201 or IFVp195 and disease state, intestinal fluid accumulation ratios (FAR) and recovery of *V. parahaemolyticus* determined at 15-, 38- and 120-hours post infection (HPI). [A] Disease, evident as diarrhoea, was recorded for individual animals. [B]Fluid accumulation ratios (FAR) were represented as mean ± standard deviation of all rabbits within the group. [C] Concentrations of *V. parahaemolyticus* recovered in intestinal homogenates taken from the proximal (I1), mid (I2) and distal regions (I3) of the small intestine.

(Meparambu Prabhakaran et al., 2022). Presence of f237 and VPaI regions, shown to be restricted to pandemic O3:K6 *V. parahaemolyticus* strains (Nasu et al., 2000) (Hurley et al., 2006), in non-toxigenic (*tdh*$^-$ and *trh*$^-$) and non-O3:K6 strains suggested high horizontal gene transfer rates in environment between *V. parahaemolyticus* strains. Presence of these regions in non-toxigenic strains, corroborated with previous studies (Ronholm et al., 2016), arise questions about their implication in environmental fitness rather than in pathogenicity. Moreover, in our study, ORFs of f237 are present in three strains expressing varying virulent phenotypes in larvae assays (IFVp18 highly virulent, IFVp136 intermediate and IFVp203 poorly virulent) and no correlation can be made between presence of VPaI regions in strain genomes and their virulence in larvae. Collectively, virulence genes, prophages and pathogenicity islands are important for *V. parahaemoluticus* fitness, providing genetic adaptability in response to changing environmental conditions.

The environmental *V. parahaemolyticus* strains, IFVp201 and IFVp195, showed contrasting phenotypes when tested in the two infection models. IFVp201 (*tdh3*$^+$ *trh1*$^+$ T3SS2β$^+$) appeared highly virulent in infant rabbits but caused only 28% mortality in larvae whereas IFVp195 (*tdh1*$^+$ T3SS2α$^+$) appeared avirulent in rabbits and caused 78% mortality in larvae. The avirulent nature of IFVp195 in rabbits was surprising given the *tdh*$^+$ T3SS2α phylotype of this strain and the previous results using RIMD2210633 (Ritchie et al., 2012). Whether variation in *tdh* allele, T3SS2 effector profile or other genetic changes explain this finding remains to be determined. It was also notable that infection with IFVp201, an T3SS2β phylotype strain that shares the same hemolysin profile as the highly pathogenic ST36 (North-West Pacific) lineage (Martinez-Urtaza et al., 2013; McLaughlin et al., 2005), yielded disease phenotypes more severe than those seen for the *tdh*$^+$ T3SS2α pandemic reference strain. For example, intestinal fluid accumulation in IFVp201 and RIMD2210633 infected animals was 0.69 ± 0.44 and 0.29 ± 0.13 (Ritchie et al., 2012), respectively. Indeed, the gross appearance

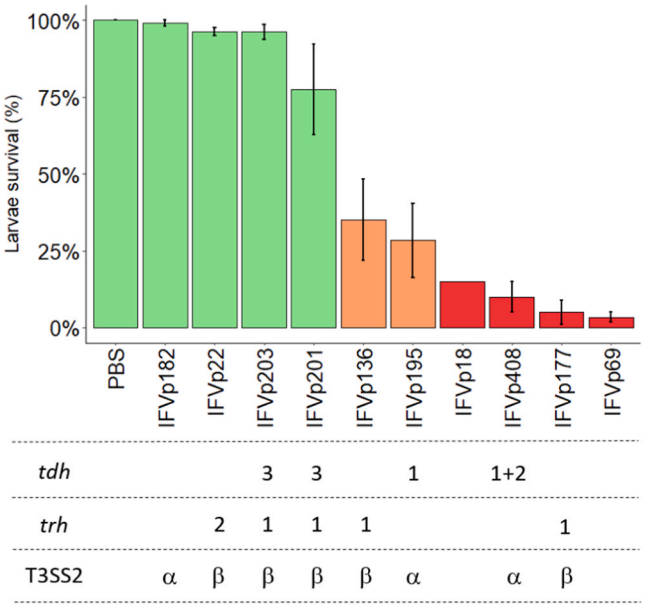

Fig. 6. *G. mellonella* larvae survival following infection with IFVp strains. Percentage of larvae survival at 24 h post-injection with approx. 5 $\times 10^6$ CFU mL^{-1} of IFVp strains. Data are represented as mean ± standard error after triplicate independent groups of 20 larvae were infected. Green: larvae survival > 75%, orange: 75% > larvae survival > 15%, red: larvae survival < 15%. Key *V. parahaemolyticus* virulence gene content for each strain is indicated below the graph. Data for IFVp5 was not determined.

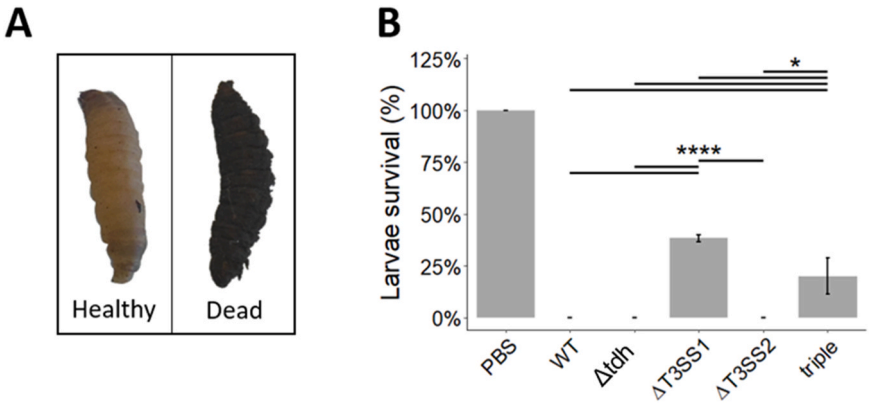

Fig. 5. *Galleria mellonella* infections with RIMD2210633 and genetic derivatives. (A) Images of healthy and dead larvae. (B) Percentage of survival of larvae at 24 h post-injection with approx. 1$\times 10^7$ CFU mL^{-1} of RIMD2210633 and mutants. Data represented mean ± standard error after triplicate independent groups of 20 larvae were infected.

of the gastrointestinal tract appeared similar to that seen in rabbits infected with AM19226, a T3SS2α-encoding non-O1, non-O139 strain of *V. cholerae* (Shin et al., 2011). Most of the disease caused by RIMD2210633 and AM19226 can be attributed to the functional activity of T3SS2α (Ritchie et al., 2012; Zhou et al., 2013); similarly, disease in T3SS2β-encoding variants has been broadly ascribed to the functional activity of T3SS2β (Okada et al., 2009). While nine effectors have now been identified for T3SS2 (Matsuda et al., 2020), their biological impact is usually described in the T3SS2α strain lineage and a broader evaluation of their role in T3SS2β-encoding strains is urgently needed to help inform risk.

Disease outcomes associated with the two model hosts did not appear to correlate, however, comprehensive assessment of all IFVp isolates in the mammalian host was beyond the scope of the project. Differences in disease outcomes may reflect the physiological challenge encountered by the bacterium due to the different routes of infection (oral *vs* direct injection) or host developmental stage. It is also possible that the models are complementary as the different routes may enable different aspects of *V. parahaemolyticus* pathogenicity to be studied. For example, orogastric inoculation of germfree mice revealed roles for T3SS2 (Yang et al., 2019), whereas intraperitoneal injection of the same host found roles for T3SS1 (Hiyoshi et al., 2010). Forced feeding of *G. mellonella* larvae may provide a viable non-mammalian alternative (Ramarao et al., 2012), although differences in the structure and composition of microbiota within hosts should be taken into account (Kostic et al., 2013). Finally, we were unable to corroborate a role for *mutT* as a potential virulence factor of *V. parahaemolyticus* (Wagley et al., 2018) as this gene was present in all our strains.

To conclude, we recovered a range of genetically diverse *V. parahaemolyticus* from shellfish production areas, many of which contained historically recognised virulence markers. Yet phenotypic testing using two models of infection failed to agree ranking based on pathogenic potential thereby highlighting a need for fuller understanding of virulence in this species. The importance of this quest cannot be understated as current national institutions rely on the use of *tdh* and *trh* as markers of disease risk, leading to the removal of seafood/shellfish from the food chain and/or the closure of shellfish production areas (NSSP, 2017). Further studies using more diverse *V. parahaemolyticus* strains, *in vivo* models and genomic analyses are needed to identify more relevant criteria.

Author statement

The authors listed on this manuscript confirm that the work reported is original, has not been published before and is not currently being considered for publication elsewhere. The manuscript has been read and approved by all named authors and that there are no other persons who satisfied the criteria for authorship but are not listed. We further confirm that the order of authors listed in the manuscript has been approved by all of us. We understand that the Corresponding Author is the sole contact for the Editorial process. He/she is responsible for communicating with the other authors about progress, submissions of revisions and final approval of proofs.

CRediT authorship contribution statement

Alain Rince: Methodology. **Veronique Verrez-Bagnis:** Methodology, Writing – review & editing. **Jennifer M Ritchie:** Conceptualization, Data curation, Formal analysis, Funding acquisition, Investigation, Methodology, Supervision, Visualization, Writing – original draft, Writing – review & editing. **Delphine Passerini:** Methodology, Writing – review & editing. **David Richard:** Formal analysis, Investigation. **Natacha Keomurdjian:** Formal analysis, Investigation. **Christine Delbarre-Ladrat:** Methodology, Writing – review & editing. **Alexandra Hughes:** Formal analysis, Investigation. **Dominique Hervio-Heath:** Conceptualization, Data curation, Formal analysis, Funding acquisition, Investigation, Methodology, Supervision, Writing – review & editing. **Solen Lozach:** Formal analysis, Investigation. **Marion Sorée:** Conceptualization, Data curation, Formal analysis, Investigation, Methodology, Writing – original draft, Writing – review & editing.

Declaration of Competing Interest

The authors declare that they have no competing interests that could have appeared to influence the work reported in this paper.

Data availability

Data will be made available on request.

Acknowledgments

We thank Amine M. Boukerb for his advice concerning genome assembling, the LABGeM (CEA/Genoscope & CNRS UMR8030), the France Génomique and French Bioinformatics Institute national infrastructures for support within the Microscope annotation platform, and the Biomedical Research facility staff at the University of Surrey for support performing animal studies. This work was supported from several sources, DHH by the Society for Applied Microbiology (Laboratory Fellowship Grant Award) and JMR by Royal Society Award (RG120193) and a Faculty Research Support Fund Award from the University of Surrey.

Appendix A. Supporting information

Supplementary data associated with this article can be found in the online version at doi:10.1016/j.micres.2024.127744.

References

Ahn, S., Chung, H.Y., Lim, S., Kim, K., Kim, S., Na, E.J., Caetano-Anolles, K., Lee, J.H., Ryu, S., Choi, S.H., et al., 2016. Complete genome of *Vibrio parahaemolyticus* FORC014 isolated from the toothfish. Gut Pathog. *8*, 59.

Alikhan, N.F., Petty, N.K., Ben Zakour, N.L., Beatson, S.A., 2011. BLAST Ring Image Generator (BRIG): simple prokaryote genome comparisons. BMC Genom. *12*, 402.

Baba, K., Shirai, H., Terai, A., Takeda, Y., Nishibuchi, M., 1991. Analysis of the *tdh* gene cloned from a *tdh* gene- and *trh* gene-positive strain of *Vibrio parahaemolyticus*. Microbiol Immunol. *35*, 253–258.

Bacian, C., Verdugo, C., Garcia, K., Perez-Larruscain, J., de Blas, I., Cachicas, V., Lopez-Joven, C., 2021. Longitudinal study of total and pathogenic *Vibrio parahaemolyticus* (*tdh*+ and/or *trh*+) in two natural extraction areas of *Mytilus chilensis* in Southern Chile. Front Microbiol *12*, 621737.

Baker-Austin, C., Trinanes, J.A., Taylor, N.G.H., Hartnell, R., Siitonen, A., Martinez-Urtaza, J., 2013. Emerging Vibrio risk at high latitudes in response to ocean warming. Nat. Clim. Change *3*, 73–77.

Bhoopong, P., Palittapongarnpim, P., Pomwised, R., Kiatkittipong, A., Kamruzzaman, M., Nakaguchi, Y., Nishibuchi, M., Ishibashi, M., Vuddhakul, V., 2007. Variability of properties of *Vibrio parahaemolyticus* strains isolated from individual patients. J. Clin. Microbiol *45*, 1544–1550.

Brynildsrud, O., Bohlin, J., Scheffer, L., Eldholm, V., 2016. Rapid scoring of genes in microbial pan-genome-wide association studies with Scoary. Genome Biol. *17*, 238.

Camacho, C., Coulouris, G., Avagyan, V., Ma, N., Papadopoulos, J., Bealer, K., Madden, T.L., 2009. BLAST+: architecture and applications. BMC Bioinforma. *10*, 421.

Castillo, D., Perez-Reytor, D., Plaza, N., Ramirez-Araya, S., Blondel, C.J., Corsini, G., Bastias, R., Loyola, D.E., Jana, V., Pavez, L., et al., 2018. Exploring the genomic traits of non-toxigenic *Vibrio parahaemolyticus* strains Isolated in Southern Chile. Front Microbiol *9*, 161.

Champion, O.L., Wagley, S., Titball, R.W., 2016. *Galleria mellonella* as a model host for microbiological and toxin research. Virulence *7*, 840–845.

Chen, Y., Stine, O.C., Badger, J.H., Gil, A.I., Nair, G.B., Nishibuchi, M., Fouts, D.E., 2011. Comparative genomic analysis of *Vibrio parahaemolyticus*: serotype conversion and virulence. BMC Genom. *12*, 294.

Deter, J., Lozach, S., Veron, A., Chollet, J., Derrien, A., Hervio-Heath, D., 2010. Ecology of pathogenic and non-pathogenic *Vibrio parahaemolyticus* on the French Atlantic coast. Effects of temperature, salinity, turbidity and chlorophyll a. Environ. Microbiol *12*, 929–937.

Froelich, B.A., Noble, R.T., 2016. Vibrio bacteria in raw oysters: managing risks to human health. Philos. Trans. R. Soc. Lond. B Biol. Sci. *371*.

Hazen, T.H., Lafon, P.C., Garrett, N.M., Lowe, T.M., Silberger, D.J., Rowe, L.A., Frace, M., Parsons, M.B., Bopp, C.A., Rasko, D.A., et al., 2015. Insights into the environmental

reservoir of pathogenic *Vibrio parahaemolyticus* using comparative genomics. Front Microbiol *6*, 204.
Hervio-Heath, D., Colwell, R.R., Derrien, A., Robert-Pillot, A., Fournier, J.M., Pommepuy, M., 2002. Occurrence of pathogenic vibrios in coastal areas of France. J. Appl. Microbiol *92*, 1123–1135.
Hiyoshi, H., Kodama, T., Iida, T., Honda, T., 2010. Contribution of *Vibrio parahaemolyticus* virulence factors to cytotoxicity, enterotoxicity, and lethality in mice. Infect. Immun. *78*, 1772–1780.
Honda, T., Ni, Y.X., Miwatani, T., 1988. Purification and characterization of a hemolysin produced by a clinical isolate of Kanagawa phenomenon-negative *Vibrio parahaemolyticus* and related to the thermostable direct hemolysin. Infect. Immun. *56*, 961–965.
Hu, M., Zhang, Y., Gu, D., Chen, X., Waldor, M.K., Zhou, X., 2021. Nucleolar c-Myc recruitment by a Vibrio T3SS effector promotes host cell proliferation and bacterial virulence. EMBO J. *40*, e105699.
Hurley, C.C., Quirke, A., Reen, F.J., Boyd, E.F., 2006. Four genomic islands that mark post-1995 pandemic *Vibrio parahaemolyticus* isolates. BMC Genom. *7*, 104.
Iida, T., Hattori, A., Tagomori, K., Nasu, H., Naim, R., Honda, T., 2001. Filamentous phage associated with recent pandemic strains of Vibrio parahaemolyticus. Emerg. Infect. Dis. *7*, 477–478.
Jensen, R.V., Depasquale, S.M., Harbolick, E.A., Hong, T., Kernell, A.L., Kruchko, D.H., Modise, T., Smith, C.E., McCarter, L.L., Stevens, A.M., 2013. Complete genome sequence of prepandemic *Vibrio parahaemolyticus* BB22OP. Genome Announc *1*.
Jesser, K.J., Valdivia-Granda, W., Jones, J.L., Noble, R.T., 2019. Clustering of *Vibrio parahaemolyticus* isolates using MLST and whole-genome phylogenetics and protein motif fingerprinting. Front Public Health *7*, 66.
Jolley, K.A., Bray, J.E., Maiden, M.C.J., 2018. Open-access bacterial population genomics: BIGSdb software, the PubMLST.org website and their applications. Wellcome Open Res *3*, 124.
Jones, J.L., Ludeke, C.H., Bowers, J.C., Garrett, N., Fischer, M., Parsons, M.B., Bopp, C.A., DePaola, A., 2012. Biochemical, serological, and virulence characterization of clinical and oyster *Vibrio parahaemolyticus* isolates. J. Clin. Microbiol *50*, 2343–2352.
Kishishita, M., Matsuoka, N., Kumagai, K., Yamasaki, S., Takeda, Y., Nishibuchi, M., 1992. Sequence variation in the thermostable direct hemolysin-related hemolysin (*trh*) gene of *Vibrio parahaemolyticus*. Appl. Environ. Microbiol *58*, 2449–2457.
Kostic, A.D., Howitt, M.R., Garrett, W.S., 2013. Exploring host-microbiota interactions in animal models and humans. Gene Dev. *27*, 701–718.
Kumar, S., Stecher, G., Li, M., Knyaz, C., Tamura, K., 2018. MEGA X: Molecular evolutionary genetics analysis across computing platforms. Mol. Biol. Evol. *35*, 1547–1549.
Langmead, B., Wilks, C., Antonescu, V., Charles, R., 2019. Scaling read aligners to hundreds of threads on general-purpose processors. Bioinformatics *35*, 421–432.
Ludeke, C.H., Kong, N., Weimer, B.C., Fischer, M., Jones, J.L., 2015. Complete genome sequences of a clinical isolate and an environmental isolate of *Vibrio parahaemolyticus*. Genome Announc *3*.
Makino, K., Oshima, K., Kurokawa, K., Yokoyama, K., Uda, T., Tagomori, K., Iijima, Y., Najima, M., Nakano, M., Yamashita, A., et al., 2003. Genome sequence of *Vibrio parahaemolyticus*: a pathogenic mechanism distinct from that of *V cholerae*. Lancet *361*, 743–749.
Martinez-Urtaza, J., Baker-Austin, C., Jones, J.L., Newton, A.E., Gonzalez-Aviles, G.D., DePaola, A., 2013. Spread of Pacific Northwest *Vibrio parahaemolyticus* strain. N. Engl. J. Med *369*, 1573–1574.
Martinez-Urtaza, J., Powell, A., Jansa, J., Rey, J.L., Montero, O.P., Campello, M.G., Lopez, M.J., Pousa, A., Valles, M.J., Trinanes, J., et al., 2016. Epidemiological investigation of a foodborne outbreak in Spain associated with U.S. West Coast genotypes of *Vibrio parahaemolyticus*. Springerplus *5*, 87.
Martinez-Urtaza, J., Trinanes, J., Abanto, M., Lozano-Leon, A., Llovo-Taboada, J., Garcia-Campello, M., Pousa, A., Powell, A., Baker-Austin, C., Gonzalez-Escalona, N., 2018. Epidemic dynamics of *Vibrio parahaemolyticus* illness in a hotspot of disease emergence, Galicia, Spain. Emerg. Infect. Dis. *24*, 852–859.
Matsuda, S., Hiyoshi, H., Tandhavanant, S., Kodama, T., 2020. Advances on *Vibrio parahaemolyticus* research in the postgenomic era. Microbiol Immunol. *64*, 167–181.
McInerney, J.O., McNally, A., O'Connell, M.J., 2017. Why prokaryotes have pangenomes. Nat. Microbiol *2*, 17040.
McLaughlin, J.B., DePaola, A., Bopp, C.A., Martinek, K.A., Napolilli, N.P., Allison, C.G., Murray, S.L., Thompson, E.C., Bird, M.M., Middaugh, J.P., 2005. Outbreak of *Vibrio parahaemolyticus* gastroenteritis associated with Alaskan oysters. N. Engl. J. Med *353*, 1463–1470.
Meparambu Prabhakaran, D., Patel, H.R., Sivakumar Krishnankutty Chandrika, S., Thomas, S., 2022. Genomic attributes differ between *Vibrio parahaemolyticus* environmental and clinical isolates including pathotypes. Environ. Microbiol Rep. *14*, 365–375.
Nair, G.B., Ramamurthy, T., Bhattacharya, S.K., Dutta, B., Takeda, Y., Sack, D.A., 2007. Global dissemination of *Vibrio parahaemolyticus* serotype O3:K6 and its serovariants. Clin. Microbiol Rev. *20*, 39–48.
Nasu, H., Iida, T., Sugahara, T., Yamaichi, Y., Park, K.S., Yokoyama, K., Makino, K., Shinagawa, H., Honda, T., 2000. A filamentous phage associated with recent pandemic *Vibrio parahaemolyticus* O3:K6 strains. J. Clin. Microbiol *38*, 2156–2161.
NCBI (2015). BioSample: SAMN03465090.
Nishibuchi, M., Kaper, J.B., 1985. Nucleotide-sequence of the thermostable direct hemolysin gene of *Vibrio parahaemolyticus*. J. Bacteriol. *162*, 558–564.
Nishibuchi, M., Kaper, J.B., 1990. Duplication and variation of the thermostable direct haemolysin (*tdh*) gene in *Vibrio parahaemolyticus*. Mol. Microbiol *4*, 87–99.
Nishibuchi, M., Taniguchi, T., Misawa, T., Khaeomaneeiam, V., Honda, T., Miwatani, T., 1989. Cloning and nucleotide-sequence of the gene (*Trh*) encoding the hemolysin related to the thermostable direct hemolysin of *Vibrio parahaemolyticus*. Infect. Immun. *57*, 2691–2697.
NSSP (2017). Guide for the control of molluscan shellfish, U. FDA, ed.
Okada, N., Iida, T., Park, K.S., Goto, N., Yasunaga, T., Hiyoshi, H., Matsuda, S., Kodama, T., Honda, T., 2009. Identification and characterization of a novel type III secretion system in *trh*-positive *Vibrio parahaemolyticus* strain TH3996 reveal genetic lineage and diversity of pathogenic machinery beyond the species level. Infect. Immun. *77*, 904–913.
Ono, T., Park, K.S., Ueta, M., Iida, T., Honda, T., 2006. Identification of proteins secreted via *Vibrio parahaemolyticus* type III secretion system 1. Infect. Immun. *74*, 1032–1042.
Ottaviani, D., Leoni, F., Serra, R., Serracca, L., Decastelli, L., Rocchegiani, E., Masini, L., Canonico, C., Talevi, G., Carraturo, A., 2012. Nontoxigenic *Vibrio parahaemolyticus* strains causing acute gastroenteritis. J. Clin. Microbiol *50*, 4141–4143.
Page, A.J., Cummins, C.A., Hunt, M., Wong, V.K., Reuter, S., Holden, M.T., Fookes, M., Falush, D., Keane, J.A., Parkhill, J., 2015. Roary: rapid large-scale prokaryote pan genome analysis. Bioinformatics *31*, 3691–3693.
Pan, T.M., Wang, T.K., Lee, C.L., Chien, S.W., Horng, C.B., 1997. Food-borne disease outbreaks due to bacteria in Taiwan, 1986 to 1995. J. Clin. Microbiol *35*, 1260–1262.
Park, K.S., Iida, T., Yamaichi, Y., Oyagi, T., Yamamoto, K., Honda, T., 2000. Genetic characterization of DNA region containing the *trh* and *ure* genes of *Vibrio parahaemolyticus*. Infect. Immun. *68*, 5742–5748.
Park, K.S., Ono, T., Rokuda, M., Jang, M.H., Iida, T., Honda, T., 2004. Cytotoxicity and enterotoxicity of the thermostable direct hemolysin-deletion mutants of *Vibrio parahaemolyticus*. Microbiol Immunol. *48*, 313–318.
Perez-Reytor, D., Pavon, A., Lopez-Joven, C., Ramirez-Araya, S., Pena-Varas, C., Plaza, N., Alegria-Arcos, M., Corsini, G., Jana, V., Pavez, L., et al., 2020. Analysis of the zonula occludens toxin found in the genome of the Chilean non-toxigenic *Vibrio parahaemolyticus* strain PMC53.7. Front Cell Infect. Microbiol *10*, 482.
Pineyro, P., Zhou, X., Orfe, L.H., Friel, P.J., Lahmers, K., Call, D.R., 2010. Development of two animal models to study the function of *Vibrio parahaemolyticus* type III secretion systems. Infect. Immun. *78*, 4551–4559.
Raghunath, P., 2014. Roles of thermostable direct hemolysin (TDH) and TDH-related hemolysin (TRH) in *Vibrio parahaemolyticus*. Front Microbiol *5*, 805.
Ramarao, N., Nielsen-Leroux, C., Lereclus, D., 2012. The insect *Galleria mellonella* as a powerful infection model to investigate bacterial pathogenesis. J. Vis. Exp., e4392
Rissman, A.I., Mau, B., Biehl, B.S., Darling, A.E., Glasner, J.D., Perna, N.T., 2009. Reordering contigs of draft genomes using the Mauve aligner. Bioinformatics *25*, 2071–2073.
Ritchie, J.M., Rui, H., Zhou, X., Iida, T., Kodoma, T., Ito, S., Davis, B.M., Bronson, R.T., Waldor, M.K., 2012. Inflammation and disintegration of intestinal villi in an experimental model for *Vibrio parahaemolyticus*-induced diarrhea. PLoS Pathog. *8*, e1002593.
Ronholm, J., Petronella, N., Chew Leung, C., Pightling, A.W., Banerjee, S.K., 2016. Genomic features of environmental and clinical *Vibrio parahaemolyticus* isolates lacking recognized virulence factors are dissimilar. Appl. Environ. Microbiol *82*, 1102–1113.
Sakurai, J., Matsuzaki, A., Miwatani, T., 1973. Purification and characterization of thermostable direct hemolysin of *Vibrio parahaemolyticus*. Infect. Immun. *8*, 775–780.
Salomon, D., Gonzalez, H., Updegraff, B.L., Orth, K., 2013. *Vibrio parahaemolyticus* type VI secretion system 1 is activated in marine conditions to target bacteria, and is differentially regulated from system 2. Plos One *8*.
Seemann, T., 2014. Prokka: rapid prokaryotic genome annotation. Bioinformatics *30*, 2068–2069.
Shin, O.S., Tam, V.C., Suzuki, M., Ritchie, J.M., Bronson, R.T., Waldor, M.K., Mekalanos, J.J., 2011. Type III secretion is essential for the rapidly fatal diarrheal disease caused by non-O1, non-O139 *Vibrio cholerae*. Mbio *2*, e00106–e00111.
Stamatakis, A., 2014. RAxML version 8: a tool for phylogenetic analysis and post-analysis of large phylogenies. Bioinformatics *30*, 1312–1313.
Su, Y.C., Liu, C., 2007. *Vibrio parahaemolyticus*: a concern of seafood safety. Food Microbiol *24*, 549–558.
Vallenet, D., Engelen, S., Mornico, D., Cruveiller, S., Fleury, L., Lajus, A., Rouy, Z., Roche, D., Salvignol, G., Scarpelli, C., et al., 2009. MicroScope: a platform for microbial genome annotation and comparative genomics. Database (Oxf.) *2009*, bap021.
Vezzulli, L., Colwell, R.R., Pruzzo, C., 2013. Ocean warming and spread of pathogenic vibrios in the aquatic environment. Micro Ecol. *65*, 817–825.
Wagley, S., Borne, R., Harrison, J., Baker-Austin, C., Ottaviani, D., Leoni, F., Vuddhakul, V., Titball, R.W., 2018. *Galleria mellonella* as an infection model to investigate virulence of *Vibrio parahaemolyticus*. Virulence *9*, 197–207.
Wagley, S., Koofhethile, K., Wing, J.B., Rangdale, R., 2008. Comparison of *V. parahaemolyticus* isolated from seafoods and cases of gastrointestinal disease in the UK. Int J. Environ. Health Res *18*, 283–293.
Wang, R., Deng, Y., Deng, Q., Sun, D., Fang, Z., Sun, L., Wang, Y., Gooneratne, R., 2020. *Vibrio parahaemolyticus* infection in mice reduces protective gut microbiota, augmenting disease pathways. Front Microbiol *11*, 73.
Wu, Q., Li, X., Zhang, T., Zhang, M., Xue, X., Yang, W., Hu, L., Yin, Z., Zhou, D., Sun, Y., et al., 2022. Transcriptomic analysis of *Vibrio parahaemolyticus* underlying the wrinkly and smooth Phenotypes. Microbiol Spectr. *10*, e0218822.
Wu, C., Zhao, Z., Liu, Y., Zhu, X., Liu, M., Luo, P., Shi, Y., 2020. Type III secretion 1 effector gene diversity among vibrio isolates from coastal areas in China. Front Cell Infect. Microbiol *10*, 301.
Xu, F., Gonzalez-Escalona, N., Haendiges, J., Myers, R.A., Ferguson, J., Stiles, T., Hickey, E., Moore, M., Hickey, J.M., Schillaci, C., et al., 2017. Sequence type 631

Vibrio parahaemolyticus, an emerging foodborne pathogen in North America. J. Clin. Microbiol *55*, 645–648.
Xu, F., Ilyas, S., Hall, J.A., Jones, S.H., Cooper, V.S., Whistler, C.A., 2015. Genetic characterization of clinical and environmental *Vibrio parahaemolyticus* from the Northeastern US reveals emerging resident and invasive pathogen lineages. J. Shellfish Res *34*, 726–727.
Yang, N., Liu, M., Luo, X., Pan, J., 2015. Draft genome sequence of Strain ATCC 17802 (T), the type strain of *Vibrio parahaemolyticus*. Mar. Genom. *24* (*Pt 3*), 203–205.
Yang, H., Santos, M.D., Lee, J., Law, H.T., Chimalapati, S., Verdu, E.F., Orth, K., Vallance, B.A., 2019. A novel mouse model of enteric *Vibrio parahaemolyticus* infection reveals that the Type III secretion system 2 effector VopC plays a key role in tissue invasion and gastroenteritis. Mbio *10*.
Yu, Y., Yang, H., Li, J., Zhang, P.P., Wu, B.B., Zhu, B.L., Zhang, Y., Fang, W.H., 2012. Putative type VI secretion systems of *Vibrio parahaemolyticus* contribute to adhesion to cultured cell monolayers. Arch. Microbiol *194*, 827–835.
Zerbino, D.R., Birney, E., 2008. Velvet: algorithms for *de novo* short read assembly using de Bruijn graphs. Genome Res *18*, 821–829.
Zhou, X., Gewurz, B.E., Ritchie, J.M., Takasaki, K., Greenfeld, H., Kieff, E., Davis, B.M., Waldor, M.K., 2013. A *Vibrio parahaemolyticus* T3SS effector mediates pathogenesis by independently enabling intestinal colonization and inhibiting TAK1 activation. Cell Rep. *3*, 1690–1702.
Zhou, X., Ritchie, J.M., Hiyoshi, H., Iida, T., Davis, B.M., Waldor, M.K., Kodama, T., 2012. The hydrophilic translocator for *Vibrio parahaemolyticus*, T3SS2, is also translocated. Infect. Immun. *80*, 2940–2947.